Nuclear Physics A408 (1983) 173–191

ONE-NUCLEON TRANSFER REACTIONS INDUCED BY ^{32}S ON ^{34}S AT E_{inc} = 90.0 AND 97.09 MeV *

B. BILWES [a], R. BILWES [a], V. D'AMICO [b], J. L. FERRERO [c], G. GIARDINA [b] and R. POTENZA [d]

[a] *Groupe des Basses Energies-Centre de Recherches Nucleaires-Strasbourg, France*
[b] *Istituto di Fisica-Università di Messina, Italy*
[c] *Istituto de Fisica Corpuscolar-Universidad de Valencia, Italy*
[d] *Istituto di Fisica-Università di Catania, Italy*

Received 1 October 1982
(Revised 2 May 1983)

Abstract: The one-proton and one-neutron transfer reactions in the interaction of ^{34}S with incident ^{32}S were studied in the 0–3.5 MeV excitation energy range of the exit nuclei. The experimental set-up (kinematic identification technique, implanted targets, etc.) has allowed an angular resolution of 0.2°, a mass resolution of 1.5% and a Q-value resolution of 0.35 MeV.

Comparison with DWBA computations using an analytical approximation for the radial integral, with insertion of suitable recoil corrections, demonstrates the absorptive direct mechanisms of the reactions, even when double excitation of residual nuclei is present. The extracted values for the products of spectroscopic factors are in very good agreement with the known values and they are confirmed by EFR-DWBA computations. The selectivities of the reaction receive about the same contributions from the nuclear structure as from the specific reaction mechanism.

E | NUCLEAR REACTIONS $^{34}S(^{32}S, ^{31}P)$, $(^{32}S, ^{33}S)$; E = 90, 97.09 MeV; measured $\sigma(\theta)$; deduced reaction mechanism. ^{35}Cl, ^{31}P, ^{33}S deduced product spectroscopic factors. Analytical approximation of EFR-DWBA. Enriched target.

1. Introduction

Since the advent of tandem accelerators people have studied the elastic and inelastic scattering of heavy ions and transfer reactions induced by them [1,2]. However, the greatest part of work refers to reactions induced by ions with mass $A_{inc} \leqq 20$. Some works have been published on the elastic scattering between ions of higher mass [1,3–11], but with the exception of a very few special cases [3–8] the whole region of medium-mass nuclei in collision is unexplored. Furthermore, data on transfer reactions are rare [12] in this latter region of projectile and target masses, as are data on inelastic scattering [11,13]. In addition, experiments on quasi-

* Work supported in part by CRNS (France), INFN and CRRNSM (Italy). IFIC (CSIC and CAICYT) (Spain).

elastic reactions between ions of medium mass can lead to a detailed study of their reaction mechanism, allowing the refinement of new analytical methods of approximation to DWBA and CCBA computations.

From the experimental point of view, in fact, using projectile and target nuclei with $24 \leqq A \leqq 65$ it is possible, though not easy, still to obtain enough resolution in mass, angle and energy to separate transitions to single levels of the residual nuclei [13, 14]). Using the technique of the kinematic identification of the exit particles, we could study the transitions to the low-lying levels of the residues in the one-nucleon transfer reactions

(a) $^{34}S + ^{32}S \rightarrow ^{31}P + ^{35}Cl$ $(Q_{00} = -2.49$ MeV),

(b) $^{34}S + ^{32}S \rightarrow ^{33}S + ^{33}S$ $(Q_{00} = -2.77$ MeV).

The description of the experimental method, the excitation energy spectra and the angular distributions are given in sect. 2.

From the theoretical point of view, we note that the transfer of a few nucleons between heavy ions is essentially a direct process. In this context the chosen mass region shows some advantages. First of all, the ratio $\Delta M/M$ is very small both for projectile and target nuclei. Then recoil effects in DWBA are expected to be small and it should be possible to treat them in a rough approximation [15]). Furthermore, the charges of the ions are sufficiently high to make the Coulomb field so strong at the distances where the quasielastic events occur that the classical trajectories passing there are practically coulombic. We can then apply to the DWBA radial integral the methods which are valid under the Coulomb barrier [16, 17]) even when the energy is well above, provided absorption quenches the transfer process at low values of the distance between the centres of the interacting nuclei. This simplifies enormously the computation and allows an immediate representation of the reaction mechanism, usually hidden in the machinery of the exact computations.

We wanted then to test the results obtained by this simplified DWBA theory and we made the "corresponding" EFR-DWBA computation for the one-proton transfer reaction. For this it was necessary to find the optical parameters to be used in the computations, and these were found essentially by taking advantage of the semiclassical connection between phase shifts and potentials. We have chosen this way in order to obtain a coherent frame of connection between "exact" and approximate computations. In sect. 3 we summarize the methods used and give the results obtained.

Sect. 4 is devoted to a general discussion of the results, together with the conclusions.

2. Experimental procedure and results

Targets of $\sim 3\,\mu g/cm^2$ of ^{34}S implanted on thin carbon foils ($20\,\mu g/cm^2$ thick) were bombarded by ^{32}S ions accelerated by the Tandem accelerator of the Centre de Recherches Nucleaires in Strasbourg (CRNS). The targets were prepared in collaboration with the group of the Laboratoire BERNAS of ORSAY and were carried out in that laboratory.

2.1. PARTICLE IDENTIFICATION SYSTEM

To identify the mass of the detected particles, we used the kinematic identification technique[3, 18, 19]) proposed in ref.[20]). Two position-sensitive detectors, supplied by the technical group of the CRNS, were placed in front of the target, one on each side of the beam direction, in such a way that they could be rotated conjointly around the target. The relative angle between their centres was fixed at a value of 89°. The detectors were 50 mm long and 10 mm high; their centres were placed 160 mm from the target. One complete angular distribution was obtained in three runs.

The angular calibration of the detectors was obtained by alternately placing a ten-slit grid[18]) in front of them. The slits were 0.2 mm wide and the distance from one to the next was 4 mm; the grid was placed at about 1 cm from the surface of the detector. Furthermore, the angular correlation between the two particles emitted in the elastic scattering of the beam supplied an independent control of the angles.

The coincident pulses produced in the detectors were sent to the HP 2100 computer after digitalization, and finally registered on a tape. The tape was subsequently used for the off-line analysis of the experiments. Fig. 1 shows the block diagram of the system. The codes for the analysis were developed starting from those supplied by Kalinsky[18]).

With the geometrical configuration chosen, a very high fraction of the pulses produced in one of the detectors by two-body reactions between ^{34}S and ^{32}S were obviously coincident with the pulses from the same reactions in the other detector. The contributions of random coincidences and eventual three-body reactions were actually completely negligible.

The mass resolution of the system was about 1.5%, thus allowing us to resolve very well the pulses given by the reactions of transfer of one and two nucleons among them. Some care, on the other hand, was necessary in the analysis of the one-nucleon transfer events. In fact, the tail of the adjacent very high elastic peak in the mass spectra extended into the region of the one-nucleon transfer peak (about 10000 times lower). However, due to the very high angular precision, the error produced by the selection method in this partially contaminated region was, within the statistical errors reported in the figures, in any case not more than 5%.

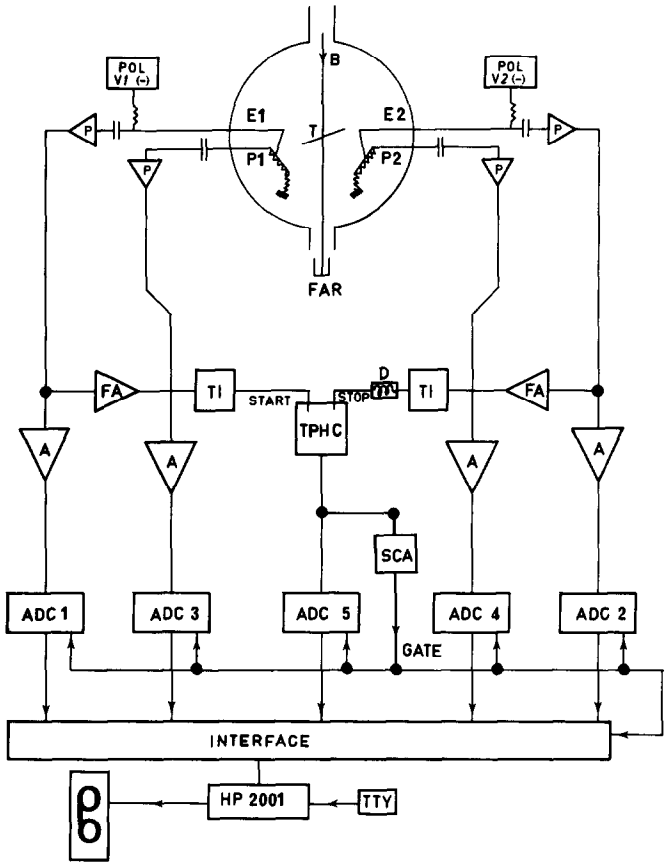

Fig. 1. Block diagram of the experimental set-up. FA: fast amplifier; P: preamplifier; A: amplifier; TPHC: time-to-pulse-height converter; ADC: analog-to-digital converter; TI: timing; D: delay; SCA: single-channel analyzer; T: target; FAR: Faraday cup; B: beam.

The error in the laboratory angles was less than 0.2°. The total angular resolution width of the system was also $\sim 0.2°$. The data however were summed in $\Delta\theta_{\text{c.m.}} = 2°$ intervals (which correspond to $\Delta\theta_{\text{lab}} \simeq 1°$) due to the low statistics.

From the kinematic relations between angles, energies and masses, one can extract directly the Q-value of the reaction from which each pair of detected particles was produced [19, 20]). A characteristic of this technique is the fact that the resolution in the measured Q-value is independent of the energy resolution of the detectors, but depends only on the angular resolution of the system. This is a great advantage which increases with incident energy and decreases with increasing masses of the residues (due to the angular spread of the ions going through the target). In the present case, the resolution width ΔQ was of about 350 keV for the low-lying levels of the residues.

2.2. EXPERIMENTAL RESULTS

2.2.1. Angular distributions. Fig. 2 shows the Q-value spectra at $E_{lab} = 90$ MeV for the reactions studied. The groups for which we measured angular distributions are indicated by broken lines. By comparison with the level schemes of the exit nuclei, drawn on the top of the spectra, we observe some selectivity and, for some groups, a probable superposition of different combinations of states of the two nuclei.

The measured cross sections of the one-proton transfer (reaction (a)) and the one-neutron transfer (reaction (b)) are given in figs. 3 and 4 at $E_{inc} = 90.00$ and 97.09 MeV, respectively. One can note the characteristic bell shape of the one-nucleon transfer angular distributions (the symmetry in the one-neutron transfer is due to the identity of the emitted particles). This form is clearly indicative of a direct mechanism, as we expected. The forward peaks of the angular distributions of these reactions are always at more forward angles with respect to the quarter-

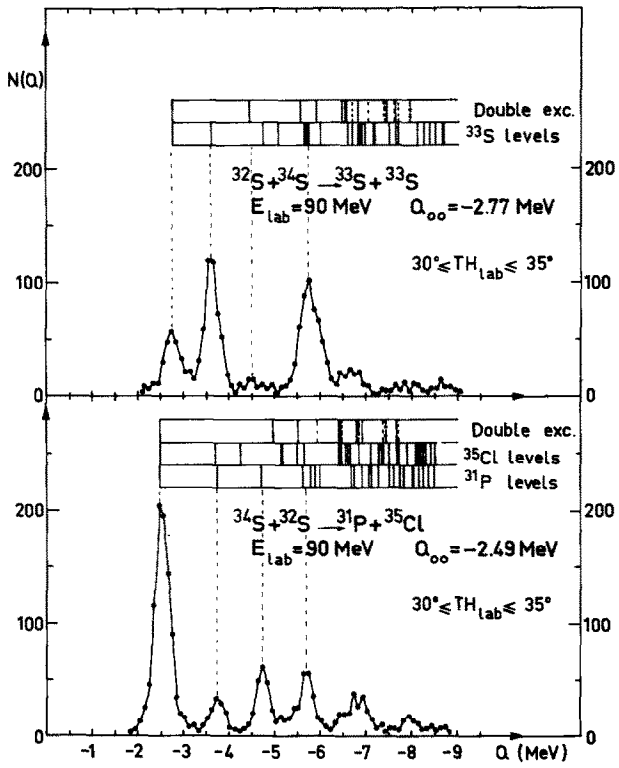

Fig. 2. Q-value spectra for the one-nucleon-transfer reactions induced by ^{32}S on ^{34}S. The peaks observed can be compared to the level schemes of each nuclei, in the case where only one nucleus is left in an excited state, or to the Q-values calculated when the two nuclei are left in excited states (double excitation).

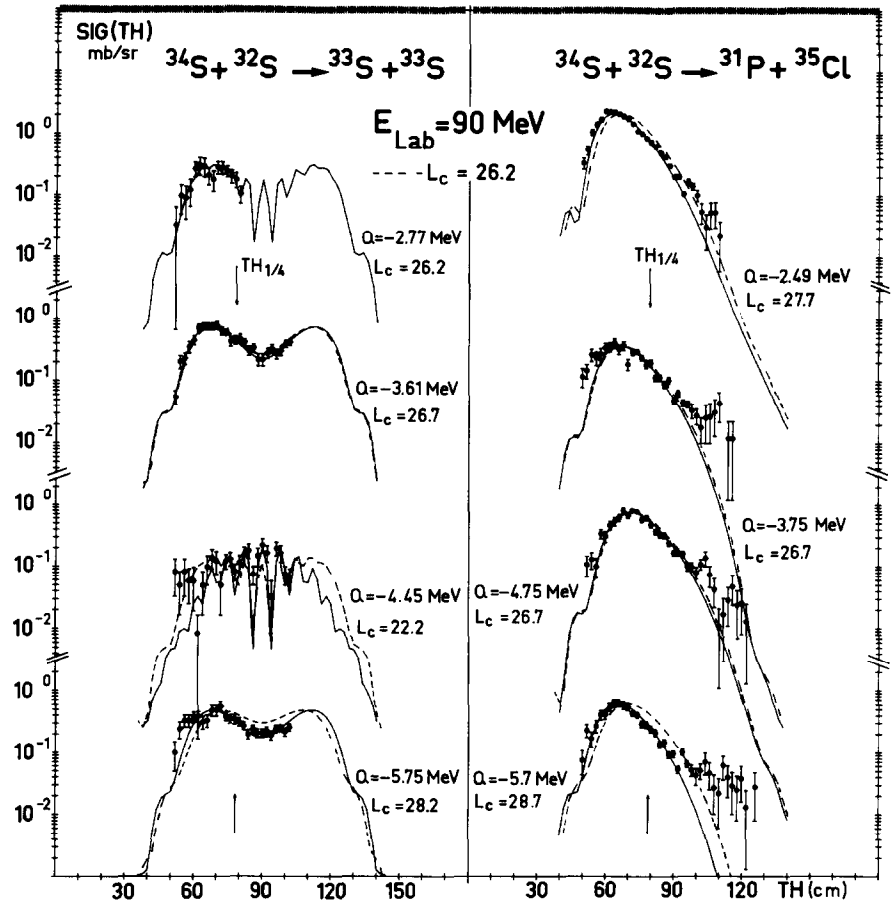

Fig. 3. Differential cross sections for the first four groups observed in the one-neutron ($^{32}S+^{34}S \rightarrow ^{33}S+^{33}S$) and in the one-proton transfer ($^{32}S+^{34}S \rightarrow ^{31}P+^{35}Cl$) at E_{inc} = 90 MeV. The approximate DWBA curves (code APPROX) are drawn on the experimental data. The broken curves are computed using S-parameters deduced from elastic scattering data (table 1). The full curves are obtained by fitting the transfer experimental data. The deduced values of l_c (denoted L_c) are indicated for each curve.

point angle in the corresponding elastic scattering angular distributions (indicated as $TH_{\frac{1}{4}}$ in figs. 3 and 4). The latter are shown in fig. 5. In the hypothesis of small nuclear refraction, this shift is indicative of the fact that the great part of the transfer process takes place when nuclei are far from interpenetrating.

Due to the very good angular resolution of the technique used, we succeeded in detecting the oscillations superimposed on the smooth trend of the experimental data, appearing essentially at backward angles of the one-proton transfer or at all angles in the case of the transitions producing both ^{33}S nuclei in the same state in the one-neutron transfer. These latter oscillations are related essentially to the

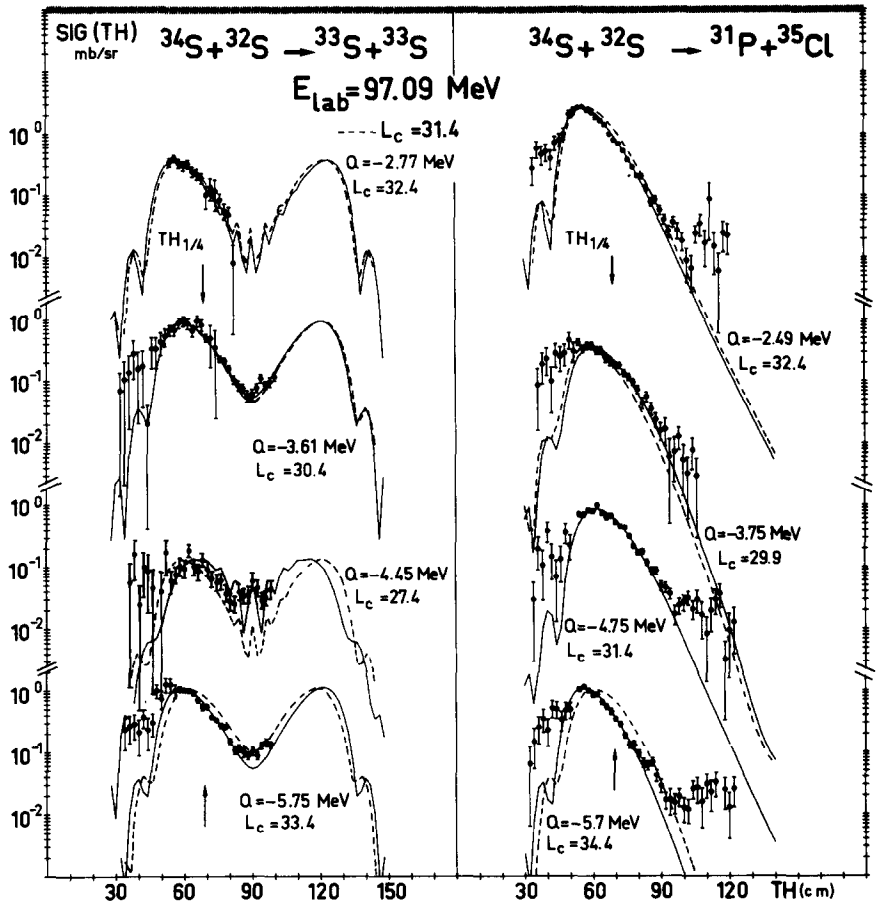

Fig. 4. As for fig. 3, but with E_{inc} = 97.09 MeV.

identity of the emitted particles. The former ones, on the contrary, seem to be related to triton transfer which can be present and interfere with the main transfer of one proton. However, its contribution in the region of the main peak is small and we have neglected it in the theoretical analysis.

2.2.2. Absolute values of the cross sections. Since the data on the different transfers were collected simultaneously with those on the elastic scattering, and thus with the same instantaneous thickness of the target and the same instantaneous dead time of the detecting and analyzing system, we could normalize the transfer counts to the elastic ones. The elastic counts at forward angles were normalized to the Rutherford cross sections. The normalization error is essentially due, in the whole procedure, to the fact that eventually the angles at which we normalize to the Rutherford cross section are not sufficiently forward, the

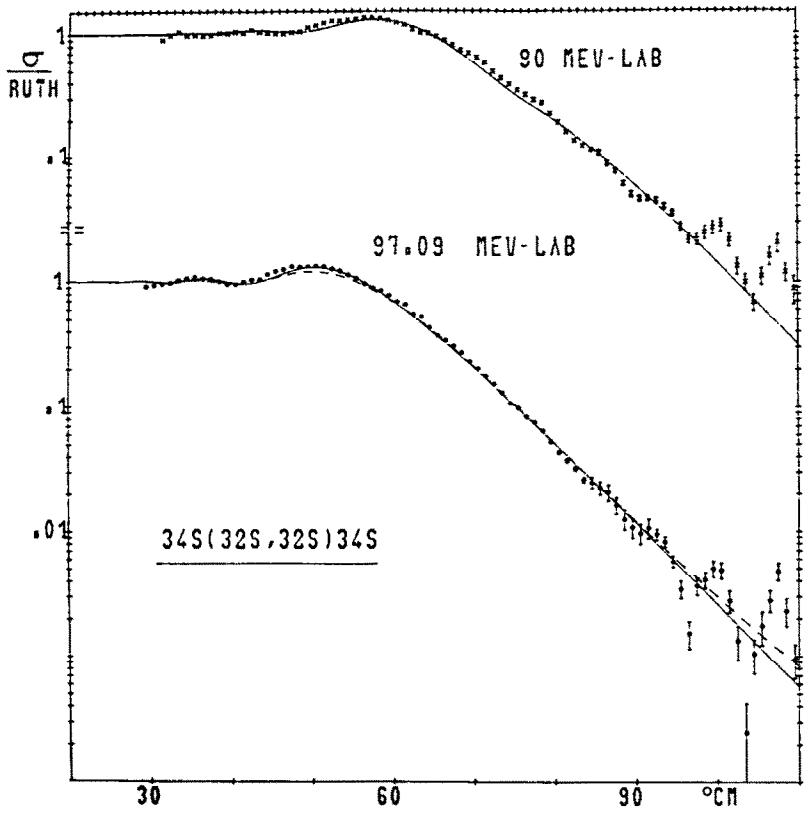

Fig. 5. Forward part of the measured elastic scattering cross section of ^{32}S on ^{34}S at $E_{inc} = 90$ and 97.09 MeV. The full curves are computed parametrizing the S-matrix. The broken one by optical model using the parameters reported in table 2.

statistical error on the elastic counts being negligible. However, due to the Fresnel form of the ratio $\sigma_{el}/\sigma_{Ruth}$, with small forward oscillations, the total normalization errors are estimated at not more than 3%.

3. Theoretical analysis of the data

3.1. DISTANT NUCLEI APPROXIMATION TO EFR-DWBA

Assuming that absorption destroys the elastic flux up to distances well above the sum of the nuclear radii of the colliding particles, we feel entitled to use the Buttle and Goldfarb method [16, 17]) of separating the twofold DWBA radial integral into the product of the size integral $A_{l_1}(\kappa_i)$ and the radial integral $T^{l,\kappa_2}_{l_i l_f}$, where l is the transferred angular momentum, $\kappa_i = \sqrt{2\mu_i B_i}/\hbar$, l_i and l_f are the angular momenta of the relative motion, and l_1 that of the particle bound to one of the nuclei, depending on the representation.

We remember that this method is strictly valid in the case of transferred neutrons in the no-recoil approximation. However, as the same authors suggest in ref. [21]), it can be extended to the case of transfer of charged particles by substituting the true tails of the bound-state wave functions of the transferred particle with appropriate Hankel functions matching the true tails at suitable chosen distances from the bounding centres.

It is also possible, when recoil effects are not large, to correct the crude no-recoil approximation by changing slightly the wave numbers of the relative motion in the incident and exit channels, as suggested in ref. [15]). By this procedure one neglects, however, the contribution of the "unnatural" parity transitions [22]).

In this framework, we used for $A_{l_1}(\kappa_1)$ the approximate expression, given in ref. [16]):

$$A_{l_1}(\kappa_1') = (-1)^{l_1}_{l_1} \frac{\hbar}{2\mu_1} N_1 \kappa_2'^{\,l_1} \kappa_1'^{\,-(l_1+1)}, \tag{1}$$

where κ_1' and κ_2', which replace κ_1 and κ_2, are the parameters of the cited Hankel functions. For the radial integral $T^{l_i,\kappa_2}_{l_i l_f}$ we used the form suggested by Frahn [23]), based on the Sopkovich prescription:

$$T^{l_i,\kappa_2'}_{l_i l_f} = N_2 (S_{l_i} S_{l_f})^{\frac{1}{2}} I^{l_i,\kappa_2'}_{l_i l_f}(Q)/2k_i' k_f' \kappa_2', \tag{2}$$

where k_i' and k_f' are the incident and exit wave numbers corrected for recoil [15]), the $S_l = \eta_l e^{2i\delta_l}$ are the nuclear elastic matrix elements in the two channels, and $I^{l_i,\kappa}_{l_i l_f}(Q)$ is the appropriate Coulomb integral [17, 23]). The radial integral depends on the Q-value of the reaction and on the recoil through $\Delta k = k_f' - k_i'$ and $\Delta n = n_f - n_i$, the n's being the Sommerfeld parameters.

We used the semiclassical approximation reported in the appendix of ref. [23]) for $I^{l_i,\kappa_2'}_{l_i l_f}(Q)$, due to the relatively large values of $n = \frac{1}{2}(n_i + n_f)$ and of l_i and l_f. N_1 and N_2 are given by

$$N_i = u_{l_i}(r_i)/h^{(1)}_{l_i}(i\kappa_i' r_i)$$

at the chosen values of r_i.

3.2. PARAMETRIZATION OF THE ELASTIC SCATTERING MATRIX

To compute the cross sections for the reactions studied, we parametrized the elements of the elastic scattering matrix putting η_l and δ_l in the form

$$\eta_l = [1 + \exp((l_c - l)/\Delta_c)]^{-1}, \tag{3}$$

$$\delta_l = \delta_0 [1 + \exp((l - \Lambda_p)/\Delta_p)]^{-1}, \tag{4}$$

as proposed in ref. [24]). The values of the parameters l_c, Δ_p, Δ_c, Δ_p and δ_0 for the incident channel were obtained by fitting the elastic scattering $^{34}S+^{32}S$ at the same incident energies using the code DIFFRAC [24]). The curves obtained are shown in fig. 5 and the values of the fitting parameters are reported in table 1. The values of the parameters for the exit channels were deduced from those for the incident one assuming the same Δ_p in both channels, the same parameter r_{0c} (reported in table 1) for the critical radii $R_c = r_{0c}(A_1^{\frac{1}{3}}+A_2^{\frac{1}{3}}) = (1/k)[n+\sqrt{n^2+(l_c+\frac{1}{2})^2}]$ in purely Coulomb trajectories, the same diffusivity of the nuclear surface $d = (\Delta_c/k)(1-2n/kR_c)^{\frac{1}{2}}/(1-n/kR_c)$ and critical nuclear deflections $\theta_N(l_c) = 2(\mathrm{d}\delta_l/\mathrm{d}l)_{l_c}$ proportional to the wave number k of the relative motions. The DIFFRAC code contains in itself the condition that

$$\frac{\mathrm{d}\theta(l)}{\mathrm{d}l} = 2\frac{\mathrm{d}^2(\delta_l+\sigma_l)}{\mathrm{d}l^2} \neq 0 \tag{5}$$

for all values of l, so that the deflection function $\theta(l)$ has no rainbows. This is what we call weak nuclear refraction.

3.3. ANGULAR DISTRIBUTION

Although it is possible, in many cases, to approximate analytically not only the twofold radial integral, as we have actually done, but also the sum of the partial waves appearing in the expression of the cross section [23, 24]), we have preferred to do numerically this latter, to avoid loss of generality when one is at the limits of the approximation methods. This numerical computation was accomplished by the code APPROX written by us. The forms of the computed angular distributions were practically independent of the value of the transfered angular momentum l. We show in figs. 3 and 4 the curves computed using either the parameters given in table 1 (broken lines) or those obtained changing the value of l_c of the incident channel (and hence the parameters of the exit channels bound to it) to fit the experimental data (full lines). The changed l_c values are shown in the figures.

As one can see, the curves reproduce well the general trend of the experimental data but with a tendency for the broken curves to a backward shift of the main peak of the order of only a few degrees. They seem to underestimate the data at forward and very backward angles. We note that fits similar to those represented

TABLE 1

S-matrix parameters for the $^{32}S+^{34}S$ elastic scattering

E_{inc}	l_c	Δ_c	Δ_p	Δ_p	δ_0	R_c	r_{0c}
90 MeV	26.2	1.7	24.0	7.5	121	9.84	1.54
97.09 MeV	31.4	1.6	19.1	8.0	189	9.88	1.54

by the broken curves have been obtained by other authors [2, 12]) in various cases when using for the DWBA computations the same optical parameters which give a good fit to the elastic scattering.

It is interesting here to note that for the transition at $Q = -4.7$ MeV in the one-proton transfer no change in l_c was necessary to fit the data. The interference patterns in the one-neutron transfer are correctly reproduced. This interference appears particularly interesting for the transition with $Q = -4.5$ MeV, from which we deduce that the main contribution to it is given by the double excitation of both ^{33}S nuclei.

3.4. SPECTROSCOPIC FACTORS

The bound-state wave functions $u_{l_1}(r)$ and $u_{l_2}(r)$ were generated by the subroutine BSAXON of the SATURN-MARS code [25]). The points of matching for the approximating Hankel functions $h^{(1)}_{l_1}(i\kappa'_1 r)$ and $h^{(1)}_{l_2}(i\kappa'_2 r)$ were chosen at the distances $r_1 = r_0 A_1^{\frac{1}{3}} + b$ and $r_2 = R_c - r_0 A_1^{\frac{1}{3}} + 1/\kappa_2$ respectively, with b as variable parameter and $r_0 = 1.25$ fm. The values of r_2 correspond to the point from which one expects the maximum transfer contribution.

The products of the spectroscopic factors for the pure transitions to one pair of levels were obtained from the usual expression

$$\sigma_{\exp}(\theta) = C_1^2 S_1 C_2^2 S_2 \sigma_{\mathrm{DWBA}}(\theta). \tag{6}$$

The results were almost independent of the incident energy. They show little sensitivity to reasonable variations of r_2 and of the recoil corrections, while they depend on the value of r_1. Effectively to reproduce correctly the known values of $S_1 S_2$ [ref. [26])] it is necessary to choose different values of r_1 for different values of l or, as we have actually done, to take the same value of r_1 for all l and to correct empirically the l-dependence of $I^{l}_{l_i l_f}(Q)$. The expression used for this Coulomb integral contains [23]) in fact the factor

$$g_l = \sum_{m=0}^{l} \frac{(l+m)!}{(l-m)!m!} \frac{C_m}{(2\kappa'_2 \rho_{l_f})^m},$$

with $\rho_{l_f} = n + \sqrt{n^2 + (l_f + \frac{1}{2})^2}$, originating from the form of the Hankel function. The empirical correction was done by dividing each term of this sum by $2m+1$. We attribute this behaviour to the fact that the approximation involved in deriving $A_{l_1}(\kappa_1)$ is too crude in our case. With this correction the value of b in the expression giving r_1 resulted 0.94 fm for the proton transfer and 0.90 fm for the neutron transfer.

For the groups which must be considered incoherent superpositions of different transitions, we proceeded as follows. We noted that for the pure transitions the

products S_1S_2 obtained from the outlined approximated DWBA, agreed well with those obtained from the EFR-DWBA computations, of which we speak later, and those deduced from the corresponding light-particle reactions [26]).

So we considered it natural, in the case of mixed groups, to estimate that the contribution of the ith transition to $\sigma_{\exp}(\theta)$ is given by

$$\sigma_{\exp}^{(i)}(\theta) = \frac{(S_1S_2)_{\mathrm{LI}}^{(i)}\sigma_{\mathrm{DWBA}}^{(i)}(\theta)}{\sum_j (S_1S_2)_{\mathrm{LI}}^{(j)}\sigma_{\mathrm{DWBA}}^{(j)}(\theta)}\,\sigma_{\exp}(\theta), \tag{7}$$

where $(S_1S_2)_{\mathrm{LI}}$ are the products deduced from the data of ref. [26]). Then we substituted $\sigma_{\exp}^{(i)}(\theta)$ for $\sigma_{\exp}(\theta)$ in (6).

All the deduced products of spectroscopic factors are reported in table 3, together with all the normalization factors N_1 and N_2 and the relevant information on the involved levels of the residual nuclei for each transition.

3.5. TEST OF THE APPROXIMATION BY EFR-DWBA COMPUTATIONS

To obtain more reliable products of spectroscopic factors and to test generally the analytical approximation used, we performed EFR-DWBA computations of the cross sections of the $^{34}S + {}^{32}S \rightarrow {}^{31}P + {}^{35}Cl$ reaction at $E_{\mathrm{inc}} = 97.09$ MeV for all measured transitions. We used for this the SATURN-MARS I code of Tamura and Low [25]).

The optical parameters used for the incident and exit channels are given in table 2. By the way in which we deduced them, they have the following characteristics:

(i) The derivative of the real part of the nuclear phase shift at $l_c^* \approx l_c$ is equal to that obtained by (4) at l_c.

(ii) Writing $S_l^{\mathrm{op}} = e^{2i(\delta_l^{\mathrm{op}} + i\alpha_l^{\mathrm{op}})} = \eta_l^{\mathrm{op}} e^{2i\delta_l^{\mathrm{op}}}$, the maximum of $\mathrm{d}\eta_l^{\mathrm{op}}/\mathrm{d}l$ is placed at l_c^* and is equal to the maximum of $\mathrm{d}\eta_l/\mathrm{d}l$ from (3), but with the slightly changed parameters l_c^* and $\Delta_c^* \approx \Delta_c$.

(iii) The values of l_c^*, Δ_c^* and $(\mathrm{d}\delta_l^{\mathrm{op}}/\mathrm{d}l)_{l_c^*}$ for the exit channels are bound to the corresponding values for the incident channel by the rules described at the end of subsect. 3.2.

TABLE 2

Optical parameters for elastic scattering at $E_{\mathrm{inc}} = 97.09$ MeV

Channel	$E_{\mathrm{c.m.}}$	V_0 (MeV)	r_{0R} (fm)	a_R (fm)	W_0 (MeV)	r_{0I} (fm)	a_I (fm)
$^{32}S + {}^{34}S$	50.01	29.8	1.25	0.65	14.6	1.35	0.464
$^{31}P + {}^{35}Cl$	47.53	28.6	1.25	0.65	12.9	1.35	0.475
$^{31}P + {}^{35}Cl$	46.27	27.9	1.25	0.65	12.0	1.35	0.481
$^{31}P + {}^{35}Cl$	45.27	27.4	1.25	0.65	11.2	1.35	0.485
$^{31}P + {}^{35}Cl$	44.32	26.9	1.25	0.65	10.5	1.35	0.489

The values of l_c^* and Δ_c^* were adjusted to give a good fit to the elastic scattering in the incident channel. The phase shifts were computed from a series expansion of their JWKB expression stopped at the second-order derivative with respect to the optical potentials. Only the complex turning point nearest to the real axis was retained in the development. Property (ii) of the optical potentials was imposed following the results of ref.[27]). Since they are valid for energies well above the Coulomb barrier, we limited ourselves to $E_{inc} = 97.09$ MeV, since for $E_{inc} = 90$ MeV this condition is not fulfilled for all the exit channels. The elastic scattering cross section generated by the optical potentials used is given in fig. 5 as a broken curve and is practically identical to that obtained from the parametrized S_l (full curve).

The cross sections computed in EFR-DWBA are shown in fig. 6 as full curves,

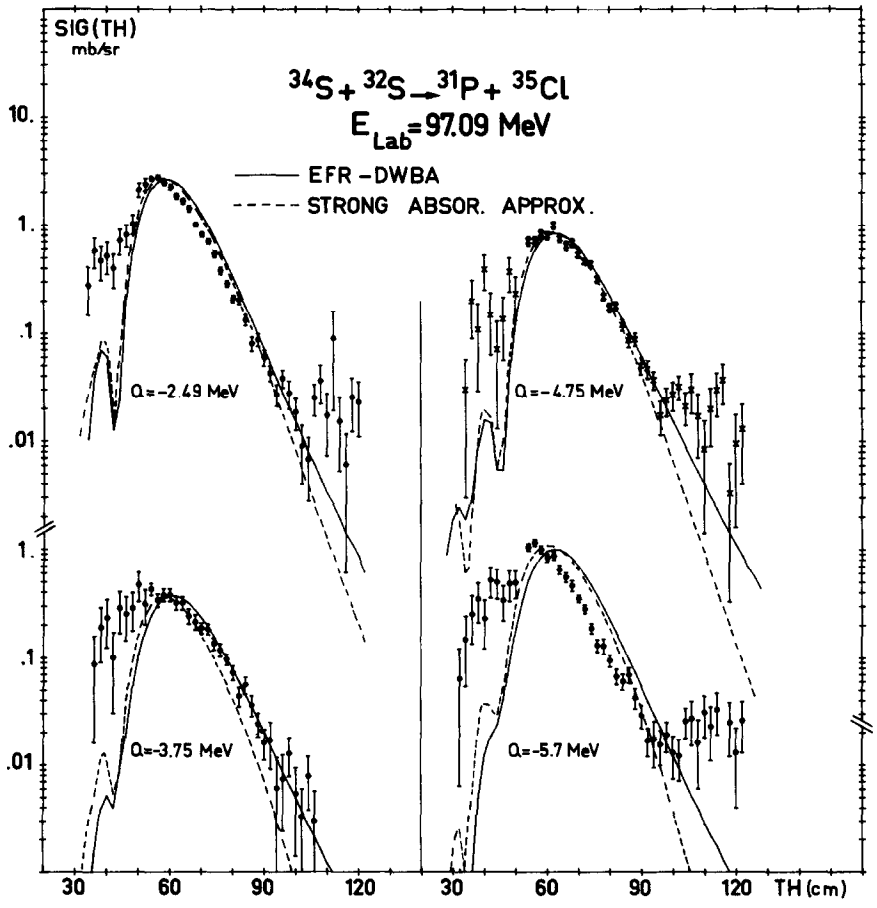

Fig. 6. Comparison between approximate DWBA computations (broken lines) and EFR-DWBA computations (full lines) for the l_c value deduced from elastic scattering measurements in both cases. The values of the optical parameters used in the SATURN-MARS code are reported in table 2.

TABLE 3

Spectroscopic factors in the $^{34}S+^{32}S$ one-nucleon transfer reactions

(a) $^{34}S+^{32}S \rightarrow {}^{31}P+{}^{35}Cl$

Q_{exp} (MeV)	^{31}P [a]		^{35}Cl [a]		l [b]	Analytic approximation to DWBA				EFR-DWBA	$(S_1S_2)_{L1}$ [e]
	E_{exc} (MeV)	nlj	E_{exc} (MeV)	nlj		N_1 [c]	N_2 [c]	S_1S_2 [d] (90 MeV)	S_1S_2 [d] (97.09 MeV)	S_1S_2 [d] (97.09 MeV)	
−2.5	0	$2s_{1/2}$	0	$1d_{3/2}$	2	17.7	3.8	2.6	2.8	3.0	2.6 ±0.6
−3.7	0	$2s_{1/2}$	1.22	$2s_{1/2}$	0	17.7	9.5	0.39	0.27	0.49	0.48±0.12
−3.7	1.27	$1d_{3/2}$	0	$1d_{3/2}$	0, 2	7.3	3.8	1.4	1.0	2.0	2.0 ±0.6
−4.7	2.23	$1d_{5/2}$	0	$1d_{3/2}$	2, 4	10.0	3.8	4.2	3.0	5.7	5.4 ±1.5
−5.7	0	$2s_{1/2}$	3.00	$1d_{5/2}$	2	17.7	1.7	0.11	0.10	0.13	0.09±0.03
−5.7	0	$2s_{1/2}$	3.16	$1f_{7/2}$	3	17.7	0.6	2.4	2.1	1.9	1.2 ±0.3
−5.7	3.13	$2s_{1/2}$	0	$1d_{3/2}$	2	29.2	3.8	0.38	0.32	0.70	0.30±0.09
−5.7	3.29	$1d_{5/2}$	0	$1d_{3/2}$	2, 4	12.0	3.8	2.2	1.4	3.1	1.5 ±0.6
−5.7	2.23	$1d_{5/2}$	1.22	$2s_{1/2}$	2	10.0	9.5	1.5	1.2		0.9 ±0.25

(b) $^{34}S + ^{32}S \rightarrow ^{33}S + ^{33}S$

Q_{exp} (MeV)	^{33}S [a]		^{33}S [a]		l [b]	Analytic approximation to DWBA				$(S_1S_2)_{LI}$ [e]
	E_{exc} (MeV)	nlj	E_{exc} (MeV)	nlj		N_1 [c]	N_2 [c]	S_1S_2 [d] (90 MeV)	S_1S_2 [d] (97.09 MeV)	
−2.8	0	$1d_{3/2}$	0	$1d_{3/2}$	0, 2	3.8	2.0	1.3	1.4	1.3 ±0.4
−3.6	0	$1d_{3/2}$	0.84	$2s_{1/2}$	2	3.8	5.4	0.24	0.23	0.5 ±0.1
−3.6	0.84	$2s_{1/2}$	0	$1d_{3/2}$	2	12.9	2.0	0.4	0.4	0.8 ±0.3
−4.5	0.84	$2s_{1/2}$	0.84	$2s_{1/2}$	0	12.9	5.4	0.25	0.15	0.3 ±0.1
−5.7	0	$1d_{3/2}$	2.87	$1d_{5/2}$	2, 4	3.8	1.0	0.7	0.7	0.7 ±0.25
−5.7	2.87	$1d_{5/2}$	0	$1d_{3/2}$	2, 4	7.4	2.0	0.08	0.1	0.1 ±0.05
−5.7	0	$1d_{3/2}$	2.93	$1f_{7/2}$	3, 5	3.8	0.42	0.06	0.08	0.06±0.05
−5.7	2.93	$1f_{7/2}$	0	$1d_{3/2}$	3, 5	4.3	2.0	0.8	1.1	1.0 ±0.3

[a]) Spectroscopic information on the involved levels of the residual nuclei for each transition contributing to the group at the given Q_{exp}.
[b]) Transferred angular momentum.
[c]) Normalization factors of the Hankel functions used.
[d]) Obtained products of the spectroscopic factors.
[e]) Products of the spectroscopic factors deduced from light-ion induced reactions [each spectroscopic factor used was the mean value among those reported in ref. [28])].

while the broken curves are those computed in the analytical approximation to DWBA with the parameters of table 1. The agreement of the two fits is very good.

The products of spectroscopic factors, which are reported in table 3 are in good agreement with those obtained in the analytical approximation and both are in agreement with those derived from literature. These results give validity to those obtained in analytical approximation for the other cases which have not been tested by EFR-DWBA computations.

4. Discussions and conclusions

4.1. REACTION MECHANISM

As we expected, the reactions studied show a clear direct mechanism with good l-matching in the whole explored range of excitation energies of the residues. This is also true for the double excitation transition at $Q = -4.5$ MeV in the $^{34}S + ^{32}S \rightarrow ^{33}S + ^{33}S$ reaction.

The pictorial simplicity in the description of the reaction mechanism obtained by the use of the analytical approximation to the DWBA allows further considerations. If the nuclear refraction is small, the fact that the decay constant of $I^{l,\kappa}_{l_i l_f}(Q)$ in (2) is much smaller than $1/\Delta_c$ in S_l implies that the reactions studied have their maximum probability when the nuclei are at distances definitely greater than the sum of the nuclear radii. Since these distances are also greater than R_c one must expect the position of the main peak in the transfer cross section to be at $\theta_0 < \theta_{\frac{1}{4}}$, as actually happens. Due to the small variations of the Q-values and of the binding energies involved for all the explored transitions, θ_0 must remain about constant, and this is also confirmed by the experiment.

Some discrepancies between theory and experiment remain however to be explained, i.e. the small backward shift in the positions of the main peaks of the theoretical cross sections and the tendency to underestimate the experimental data at forward angles, especially at the higher incident energy. They could perhaps be explained with the introduction of a certain level of surface transparency in the scattering potentials (that is an increase of the nuclear refraction). However, due to the relatively large masses of the ions involved, we think that an explanation in terms of coupling with inelastic channels is more likely, and it could give account of the apparently random peak displacements in the different transitions (the corresponding variations of l_c in figs. 3 and 4 merely represent these displacements).

The absence of shift for the transition at $Q = -4.7$ MeV in the one-proton transfer, for which selection rules forbid the coupling to the 2^+ first excited levels of the ^{32}S and ^{34}S nuclei, contributes to strenghthen this latter explanation.

4.2. SPECTROSCOPIC INFORMATION AND SELECTIVITY OF THE REACTIONS

As one sees from table 3, the absolute values of the cross sections are well given using directly the products of the known values of the spectroscopic factors obtained from the corresponding reactions induced by light ions on the nuclei concerned.

From this we can deduce some indications as far as the selectivity of the reactions is concerned.

We think that when one is dealing with transitions to individual levels of the residual nuclei, a good index of the selectivity is the relative variance of the cross sections. Remembering (6), we have, neglecting correlations,

$$v^2 = \frac{1}{n-1}\left(\frac{\sum_{i=1}[(S_1S_2)_i^2 - \langle(S_1S_2)_i\rangle^2]}{\langle(S_1S_2)_i\rangle^2} + \frac{\sum_{i=1}[\sigma^2_{\mathrm{DWBA},i} - \langle\sigma_{\mathrm{DWBA},i}\rangle^2]}{\langle\sigma_{\mathrm{DWBA},i}\rangle^2}\right) \equiv v_s^2 + v_\sigma^2$$

and we can interpret v_s^2 as the selectivity originating from the spectroscopic properties of the levels involved and v_σ^2 as that originating from the specific mechanism of the reaction.

In the present case we obtained $v_s^2 = 1.0$ and $v^2 = 2.4$ and hence $v_\sigma^2 = 1.4$ for the proton transfer, and $v_s^2 = 0.54$ and $v^2 = 1.2$ and hence $v_\sigma^2 = 0.66$ for the neutron transfer. This means that, while the reactions are moderately selective, their selectivities receive about the same contributions, which are not strong, from the nuclear structure as from the reaction mechanism.

As far as the theory is concerned, the approximate DWBA formalism still requires some improvement in the estimation of the size integral $A_{l_1}(\kappa_1')$, while we think that for the values used for the projectile and target masses, the recoil effects are well taken into account with the exception of the contribution of the unnatural-parity transitions which we neglect completely. In this case, however, this contribution is really negligible, being of the order of $\mu_u/\mu \approx 3\%$ of the absolute value alone, since the forms of the angular distributions are practically independent of the value of the transferred angular momentum.

4.3. CONCLUSIONS

We can conclude as follows:

(a) In the reactions between nuclei of medium mass, the kinematic identification technique allows a good resolution of different transitions to low-lying levels of the residual nuclei.

(b) A direct one-step reaction mechanism, dominated by absorption and where the nuclear refraction is a small perturbation of the dominant coulombic one, well accounts for the experimental data obtained and also for the absolute values of the cross sections.

(c) The small recoil effects allow us to use the distant-nuclei approximation to the DWBA, which gives an impressive visualization of the process. However, further refinements are required for the estimation of the size integral if one does not want to compute it numerically.

(d) The selectivity observed in the studied reaction receives contributions about equally from the spectroscopic properties of the involved levels and from the specific properties of the reaction mechanism.

The authors wish to acknowledge Drs. I. Link and L. Kraus for their help during experiments. Two of the authors (V. D'A. and R. P.) would like to acknowledge Prof. D. Magnac-Valette, Dr. R. Seltz and the other colleagues of the Groupe des Basses Energies of the CRNS for their kind hospitality during their stays in that laboratory. We also thank Dr. A. Villari for his kind assistance for the SATURN-MARS computations.

References

1) P. E. Hodgson, Nuclear heavy-ion reactions (Clarendon, Oxford, 1978) p. 325
2) T. Tamura, T. Udagawa and M. C. Mermaz, Phys. Reports **C65** (1980) 345
3) H. Emling, R. Novotny, D. Pelte, G. Schrieder and W. Weidenmeier, Nucl. Phys. **A239** (1975) 172
4) H. H. Gutbrod, M. Blann and W. G. Winn, Nucl. Phys. **A213** (1973) 285
5) M. Richter, W. Henning, H. T. Koerner, R. Mueller, K. E. Rehm, H. P. Rother, H. Schaller and H. Spieler, Nucl. Phys. **A278** (1977) 163
6) H. Doubre, J. C. Jacmart, E. Plagnol, N. Poffe, M. Riou and J. C. Roynette, Phys. Rev. **C15** (1977) 693
7) P. Wastyn, H. Genz, M. Mutterer, A. Richter, G. Schrieder, J. C. van Staden and J. P. Theobald, Nucl. Phys. **A320** (1979) 433
8) F. Porto, S. Sambataro, K. Kusterer, Liu Ken Pao, G. Doukellis and H. L. Harney, Nucl. Phys. **A357** (1981) 237
9) Jiang Cheng-Lie, P. R. Christensen, Ole Hansen, S. Pontoppidan, F. Videbæk, D. Schüll, Shen Wen-Qing, A. J. Baltz, P. D. Bond, H. Freiesleben, F. Busch and E. R. Flynn, Phys. Rev. Lett. **B47** (1981) 1039
10) J. S. Eck, T. R. Ophel, P. D. Clark, D. C. Weisser and G. R. Satchler, Phys. Rev. **C23** (1981) 228
11) P. D. Bond, Ole Hansen, C. E. Thorn, M. J. Levine, P. R. Christensen, S. Pontoppidan, F. Videbæk, Jiang Cheng-Lie and M. J. Rhoades-Brown, Phys. Lett. **114B** (1982) 423
12) J. D. Garrett, H. E. Wegner, T. M. Cormier, E. R. Cosman, O. Hansen and A. Lazzarini, Phys. Rev. **C12** (1975) 489
13) B. Bilwes, R. Bilwes and J. L. Ferrero, Centre de Recherches Nucléaires de Strasbourg report CRN 80-01 (1981) p. 42
14) B. Bilwes, R. Bilwes, V. D. D'Amico, J. L. Ferrero and R. Potenza, Centre de Recherches Nucléaires de Strasbourg report CRN 80-01 (1981) p. 43
15) P. J. A. Buttle and L. J. B. Goldfarb, Nucl. Phys. **A176** (1971) 299
16) P. J. A. Buttle and L. J. B. Goldfarb, Nucl. Phys. **78** (1966) 409
17) D. Trautmann and K. Alder, Helv. Phys. Acta **43** (1970) 363
18) D. Kalinsky, D. Melnik, U. Smilansky, N. Trautner, B. A. Watson, Y. Horowitz, S. Mordechai, G. Baur and D. Pelte, Nucl. Phys. **A250** (1975) 364
19) R. Wieland, R. Stokstad, A. Gobbi, D. Shapira, L. Chua, M. W. Sachs and D. A. Bromley, Phys. Rev. **C9** (1974) 1474
20) H. Emling, R. Novotny, D. Pelte and G. Schrieder, Nucl. Phys. **A211** (1973) 600

21) P. J. A. Buttle and L. J. B. Goldfarb, Nucl. Phys. **A115** (1968) 461
22) N. K. Glendenning and M. A. Nagarajan, Nucl. Phys. **A236** (1974) 13
23) W. E. Frahn, Phys. Rev. **C21** (1980) 1870
24) W. E. Frahn and K. E. Rehm, Phys. Reports **C37** (1978) 1
25) T. Tamura and K. S. Low, Comp. Phys. Comm. **8** (1974) 349
26) P. M. Endt, Atom. Nucl. Data Tables **19** (1977) 23
27) W. E. Frahn, Nucl. Phys. **A302** (1978) 281